Catalysis Science & Technology

Accepted Manuscript

This article can be cited before page numbers have been issued, to do this please use: S. Khan, L. Yang, Y. Feng, M. Cheng, N. Ahmad and G. Zhang, *Catal. Sci. Technol.*, 2026, DOI: 10.1039/D5CY01487E.

ROYAL SOCIETY OF CHEMISTRY

rsc.li/catalysis

View Article Online
DOI: 10.1039/D5CY01487E

Electronic Structure Modulation of Mo-Doped NiO/Ni Bifunctional Electrocatalyst for Efficient Urea-Assisted Water Splitting

*Shahid Khan [a], Yang Lina [a], Yafei Feng [a], Mingyu Cheng [a], Nazir Ahmad [a] and Genqiang Zhang[a]**

a. Hefei National Research Center for Physical Sciences at the Microscale, CAS Key Laboratory of Materials for Energy Conversion Department of Materials Science and Engineering, University of Science and Technology of China, Hefei, Anhui 230026, P. R. China.

* Corresponding author: gqzhangmse@ustc.edu.cn;

Keywords: Urea oxidation reaction, hydrogen evolution reaction, electronic structure modulation, bifunctional catalyst, electrodeposition, urea-assisted water splitting

View Article Online
DOI: 10.1039/D5CY01487E

ABSTRACT

Urea oxidation-assisted hydrogen production provides an energy-efficient and sustainable alternative to conventional water electrolysis by significantly reducing the required cell voltage. However, developing bifunctional catalysts with high activity, long-term stability and bifunctionality remains an ongoing challenge. Here, the electronic structure of NiO/Ni is precisely modulated through molybdenum (Mo) incorporation, enabling simultaneous enhancement of the hydrogen evolution reaction (HER) and urea oxidation reaction (UOR). The resulting Mo-NiO/Ni catalyst, obtained *via* a simple electrodeposition followed by annealing approach, exhibits outstanding activity and durability, requiring cell voltages of 1.33 and 1.62 V to achieve 10 and 100 $mA \cdot cm^{-2}$, respectively, for overall urea electrolysis, which are 170 and 200 mV lower than those of overall water electrolysis under the same conditions. Density functional theory (DFT) calculations reveal that Mo doping optimizes the electronic configuration of NiO/Ni, lowers the activation barrier of urea dehydrogenation and approached thermoneutral hydrogen adsorption. This work demonstrates an effective electronic structure engineering strategy for designing efficient bifunctional catalysts toward low-energy hydrogen production coupled with urea degradation.

View Article Online
DOI: 10.1039/D5CY01487E

1. INTRODUCTION

Urea-assisted water splitting is emerging as an efficient and sustainable strategy for green hydrogen production.(1) Compared with conventional steam reforming and coal gasification, electrocatalytic water splitting offers advantages of zero carbon emissions, high product purity, and low cost.(2) Replacing the sluggish, high-potential oxygen evolution reaction (OER, 1.23 V) with the UOR, (0.37 V vs. RHE) can markedly reduce the energy input required for hydrogen generation.(3-9) However, the complex six-electron-transfer pathway and multiple intermediates in UOR still limit practical urea-assisted H_2 production, (6, 10, 11) highlighting the need for highly active bifunctional electrocatalysts to overcome kinetic barriers and enable efficient hydrogen generation.

Noble-metal catalysts such as Pt, IrO_2, and RuO_2 exhibit excellent intrinsic activity toward both HER and UOR. However, their high cost, scarcity, and limited long-term stability severely hinder large-scale deployment in sustainable hydrogen production.(12-14) Consequently, intensive efforts have focused on developing efficient, naturally occurring, inexpensive metal-based catalysts, particularly bifunctional systems for HER and UOR. To date, a variety of cheap transition composed of metal catalysts (oxides, hydroxides, sulfides, nitrides, selenides, phosphides, etc.) are currently explored for water and electrolysis.(15-20) Among these, heteroatom doping has proven especially effective, as it can modulate the d-band center, increase the density of states adjacent the Fermi level, and thereby optimize intermediate adsorption and electron transfer.(21, 22). Constructing nitride-hydroxide and oxides heterostructure such as NiFe-LDH/Ni_3N and NdNiO-NiO interfaces, as well as introducing C-doping into NiO have been demonstrated to enhance electrochemical performance by facilitating charge transfer, promoting active NiOOH formation and modulating local coordination environments.(23-25) For instant

View Article Online
DOI: 10.1039/D5CY01487E

Zhao *et al*. constructed a NiFe-LDH/Ni_3N heterostructure that enables rapid electron transfer and stabilizes active NiOOH species, markedly improving the HER and UOR efficiency. Their findings emphases the importance of nitride-hydroxide interfacial coupling in tuning electronic structure and enhancing catalytic performance.(23) Rao *et al.* designed a $NdNiO_3$-NiO heterostructure interface that promotes charge redistribution and accelerates NiOOH formation, significantly enhancing UOR activity.(24) *Kou et al.* indicated that C-doped NiO might alter the local structure of NiO and diminish the Ni coordination number, hence enhancing H^* adsorption.(25) In addition, Ni, Co, and Mo-based compounds are widely investigated HER/UOR catalysts due to their suitable electronic configurations, natural abundance, and low cost. (6, 26-30) Inspired by these insights, incorporating foreign atoms into transition metal oxides offers a practical strategy to optimize their electronic structure for bifunctional electrocatalysis, nevertheless, Mo-doped NiO/Ni interfaces designed as truly bifunctional catalysts for both HER and UOR, supported by combined experimental and DFT evidence of Mo-induced electronic modulation, remain largely underexplored.

In this work, we report a molybdenum-doped NiO/Ni (Mo-NiO/Ni) bifunctional electrocatalyst grown on nickel foam (NF) by simple electrodeposition followed by annealing. Unlike bulk Ni-Mo-O/$NiMoO_x$ catalysts (e.g., $NiMoO_4$/$NiMoO_x$), our material is a Mo-doped NiO/Ni interfacial architecture where Mo primarily acts as an electronic modulator of the NiO/Ni interface rather than forming a separate mixed-oxide phase.(31-33) By incorporating Mo to tune the electronic structure at the NiO/Ni interface, the catalyst is designed to efficiently promote both the HER and the UOR in alkaline media using only earth-abundant, low-cost components. Importantly, it can deliver 10 and 100 $mA \cdot cm^{-2}$ at 1.33 and 1.62 V under two-electrode configuration for urea electrolysis, respectively, which are superior as compared to overall water

View Article Online
DOI: 10.1039/D5CY01487E

splitting 1.5 V and 1.82 at 10 and 100 mA·cm^{-2}. We propose that Mo incorporation tailors the local coordination and charge distribution, improving conductivity, increasing the density of accessible active sites, approaching thermoneutral hydrogen adsorption, and lowering the energy barrier for urea dehydrogenation, thereby enabling urea electrolysis at reduced cell voltages with sustained long-term stability.

2. RESULTS AND DISCUSSION

2.1. Synthesis and characterization

The Mo-NiO/Ni catalyst was fabricated through a one-step electrodeposition strategy as depicted in **Figure 1a,** followed by annealing in Ar/H_2 atmosphere at 450 °C for 2 hours. Unless otherwise stated, all electrodes were prepared on identical NF pieces (1 × 1 cm^2) using the same electrodeposition parameters (-3 V, 20 min) and the same exposed geometric test area (0.25 cm^2), ensuring direct comparability. NiO/Ni were synthesized using the same technique but without adding dopant source. The crystalline structure of the prepared samples was characterized using X-ray diffraction (XRD) technique. As shown in **Figure 1b**, all the diffraction peaks of both samples attribute to NiO (JCPDS card No. 71–1179) with no impurity phases detected (e.g., crystalline $NiMoO_4$/$NiMoO_x$). The reflections from the Ni foam substrate are also present but are not labeled for clarity, the peaks from the deposited layer are indexed to NiO. The microstructures of both samples were studied using field-emission scanning electron microscopy (FESEM), transmission electron microscopy (TEM), and high-resolution TEM (HRTEM). FESEM images of pristine NiO/Ni **Figure S1** displays a relatively smooth and compact morphology composed of loose nanoparticles, indicating limited surface roughness and lower porosity. In contrast, the Mo-NiO/Ni catalyst exhibits a markedly different surface architecture characterized by highly rough nano particles as shown in **Figure 1c,d.** This structural evolution suggests that the introduction of

View Article Online
DOI: 10.1039/D5CY01487E

Mo atom alters the nucleation and growth behavior. The TEM images of Mo-NiO/Ni further reveal the densely packed nanoparticles as depicted in **Figure 1e,f**, confirming their intimate interfacial contact. This structure revealed in TEM is expected to provide abundant exposed active sites, enhanced ion diffusion and improved electrical conductivity. The high-resolution TEM (HRTEM) image of Mo-NiO/Ni in **Figure 1g** displays lattice fringes with interplanar spacings of 0.22 and 0.21 nm, consistent with the (111) and (200) planes of NiO, respectively, in good agreement with the XRD results. Moreover, the energy-dispersive spectroscopy (EDS) mapping in **Figure 1h** confirms a uniform elemental dispersion of Nickel (Ni), molybdenum (Mo) and oxygen (O) throughout the nanoparticles, highlighting the effect of Mo doping with NiO/Ni. The Raman spectra demonstrate clear Mo-induced modifications in the NiO lattice as depicted in **Figure S2**. The Mo-NiO/Ni sample shows a strong band near 900-1000 cm^{-1} and enhanced features at 400-700 cm^{-1}, correspondingly to Ni-O-Mo interactions consistent with Ni-O-Mo bonding from highly dispersed/amorphous Mo-O species, rather than a bulk $NiMoO_x$ phase. These changes indicates that Mo doping alters the local bonding, lattice symmetry and defect structure, thereby tuning the material redox and catalytic properties.(34)

View Article Online
DOI: 10.1039/D5CY01487E

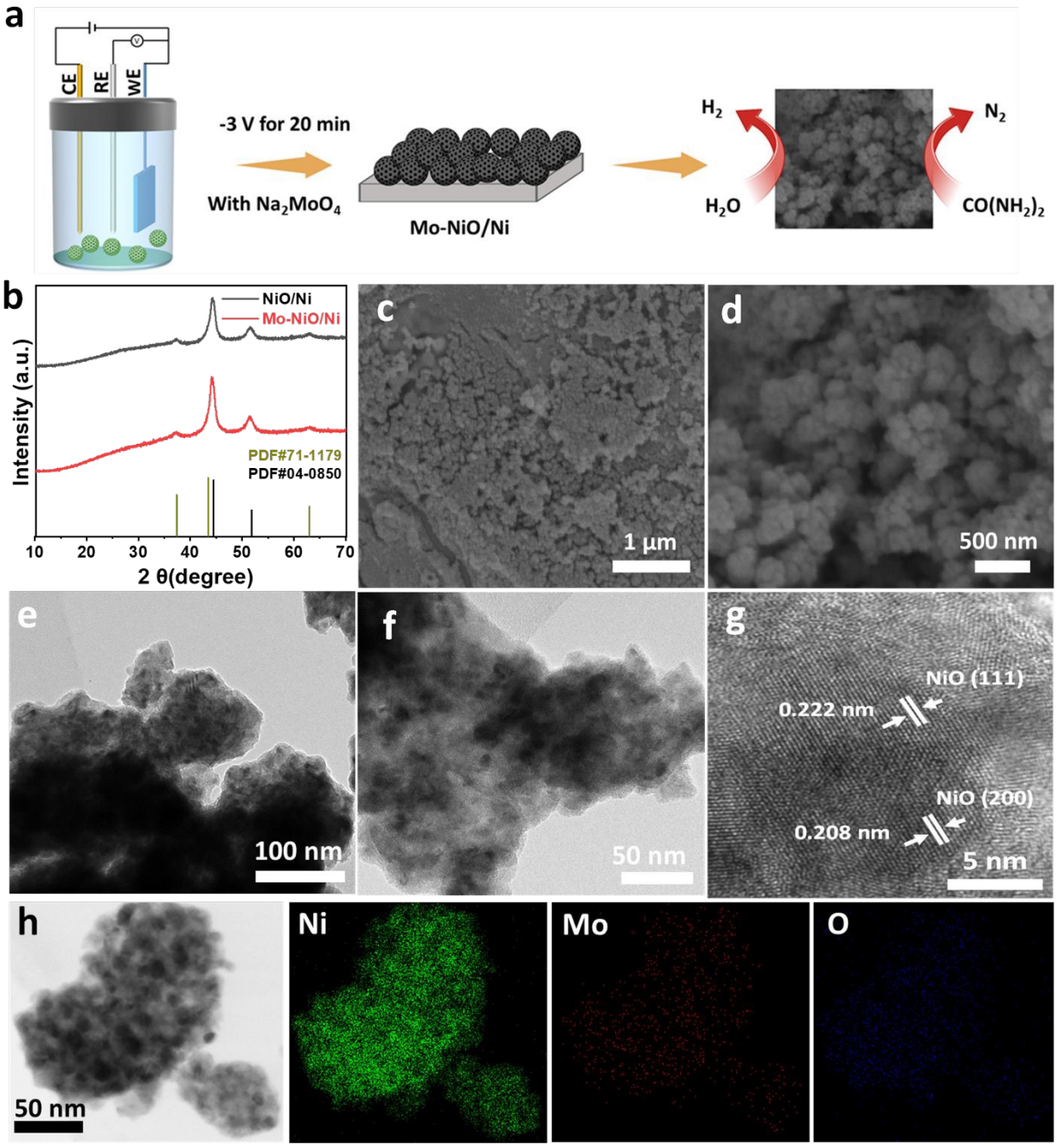

Figure 1. (a) Schematic diagram for the synthesis of the Mo-NiO/Ni catalyst. (b) XRD analysis. (c,d) SEM. (e,f) TEM. (g) HRTEM analysis. (h) Element mapping.

X-ray photoelectron spectroscopy (XPS) of NiO/Ni and Mo-NiO/Ni were analyzed to discover the influence of Mo-doping on the electronic configuration of NiO/Ni. XPS survey spectrum of Mo-NiO/Ni validates the existence of Ni, O and Mo, while the NiO/Ni confirm the

View Article Online
DOI: 10.1039/D5CY01487E

presence of Ni and O as illustrated in **Figure S3**. The high-resolution Ni 2p spectra shows that the peaks located at 852.4 and 868.3 eV are assigned to Ni^0, while the peaks located in 855.82 and 873.46 eV with satellite peaks are ascribed to the Ni^{2+} as shown in **Figure2a**.(35) Notably, the Ni 2p binding energies in Mo-NiO/Ni shift positively by 0.47 eV, which confirm that Mo doping have make changes to the electronic structure of NiO/Ni. This shift supports interfacial electronic modulation by Mo doping rather than formation of a separate bulk Ni-Mo-O ($NiMoO_x$) phase. The O1s spectrum exhibit lattice oxygen (530.86 eV) and surface-adsorbed oxygen/ hydroxyl component (532.83 eV), indicating defect concentration in Mo-NiO/Ni as depicted in **Figure 2b**.(36) The high-resolution Mo 3d spectrum **Figure 2c** demonstrates the simultaneous presence of Mo^{5+} and Mo^{6+} oxidation states in the Mo-NiO/Ni interface. The observed peaks at 229.9 eV and 233.1 eV correspond to Mo^{5+}, while those at 232.3 eV and 235.5 eV are assigned to Mo^{6+} components.(37) In the C 1s XPS spectra shows three characteristics carbon components C-C at 284.8 eV, C-O-C at 285.4 eV and C=O at 288.4 eV as illustrated in **Figure 2d**. Both NiO/Ni and Mo-NiO/Ni exhibits these peaks, indicating typical surface carbon species from air exposed or synthesis residues.(38) Such mixed-valence behavior reflects electronic coupling between Mo and Ni species, which may contribute to enhanced charge transport and catalytic activity. Collectively, these XPS results validate the successful incorporation of Mo into the NiO/Ni lattice and reveal related electronic and local structural modulation features that are conducive to enhanced bifunctional HER and UOR electrocatalysis.

View Article Online
DOI: 10.1039/D5CY01487E

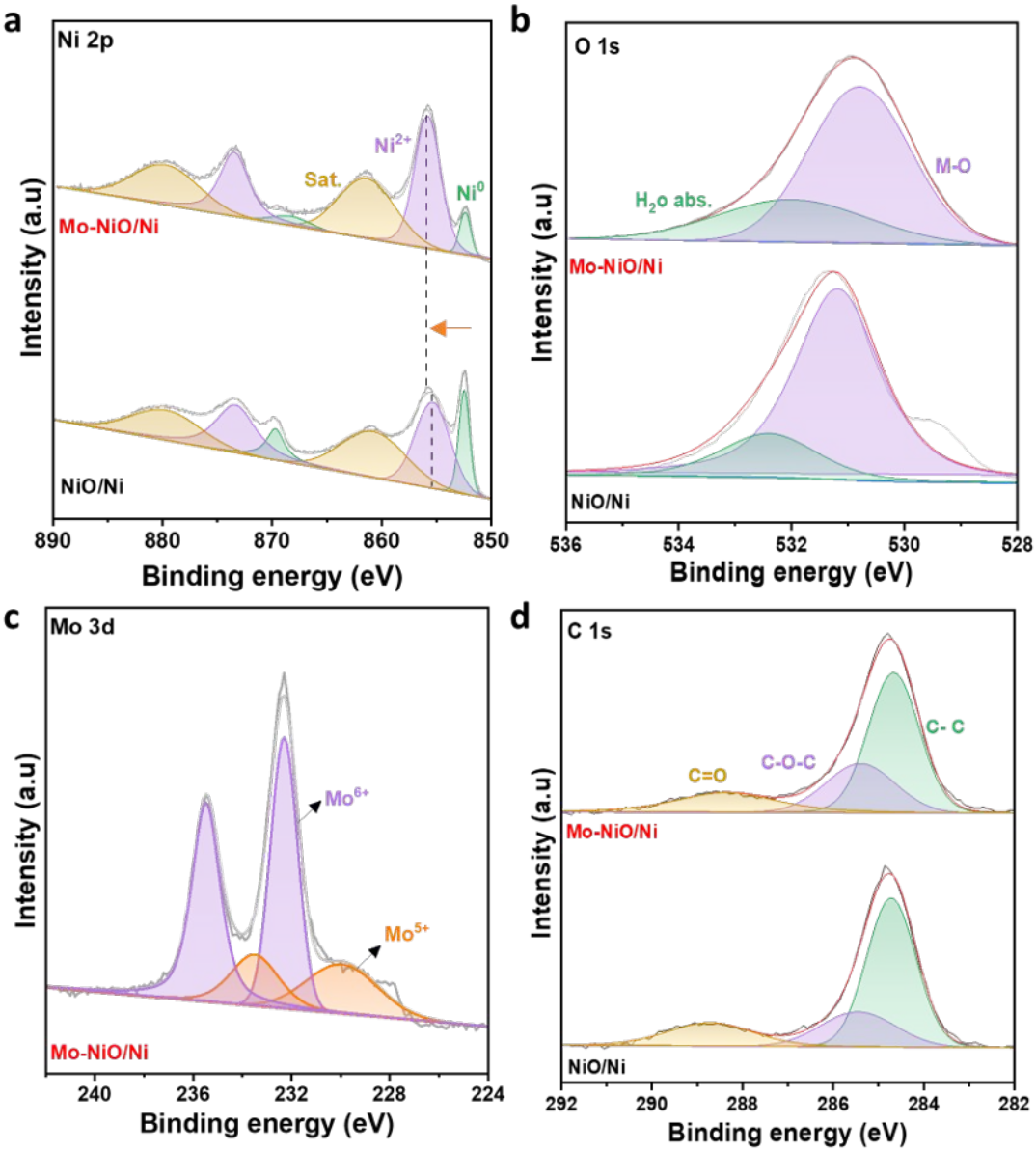

Figure 2. High resolution XPS spectra of (a) Ni2p, (b) O 1s (c) Mo 3d and (d) C 1s.

2.2 Electrochemical study of HER

To evaluate the impact of Mo doping on the polarization curves of NiO/Ni, the HER activity of the as-prepared catalysts was initially assessed employing a distinctive three electrode configuration in 1 M KOH. The Hg/HgO electrode served the reference, while the graphite rod was used as the counter electrode. Linear sweep voltammetry (LSV) was performed at a scan rate of 5 $mV \cdot s^{-1}$ to examine the electrocatalytic performance. To identify the optimal catalyst, we

View Article Online
DOI: 10.1039/D5CY01487E

investigated the effect of annealing temperatures on catalytic activity. Samples annealed at 400 °C, 450 °C and 500 °C were evaluated on their HER performance and electrochemical impedance spectroscopy (EIS) measurements as illustrated in **Figures S4**. Among them the catalyst annealed at 450 °C has the best HER activity. For comparison, the electrocatalytic activity of commercial Pt-C catalyst and blank NF has been analyzed. Moreover, the LSV curves of the prepared catalyst were measured as illustrated in **Figure 3a**. Notably, blank NF exhibited no electrocatalytic performance, whereas the Mo-NiO/Ni shows the better HER performance. As shown in **Figure S5**, the Mo-NiO/Ni only affords the overpotential of 51, 89, and 113 mV at current densities of 10,50, and 100 $mA \cdot cm^{-2}$, respectively, which are much lower than those of NiO/Ni (97, 185 and 228 mV, respectively). Meanwhile, the $\eta 10$ of Mo-NiO/Ni could also be compared to several recorded transition metals oxide catalysts in alkaline medium as depicted in **Table S1**. Specifically, as revealed in **Figure 3b**, the Tafel slope of Mo-NiO/Ni is (45 $mV \cdot dec^{-1}$), which is much smaller than that of NiO/Ni (87 $mV \cdot dec^{-1}$) indicating the favorable HER kinetics. Electrochemical double-layer capacitance (C_{dl}) was measured to estimate the electrochemical active surface area (ECSA) of Mo-NiO/Ni and NiO/Ni from CV's measurements as depicted in **Figure S6**. As shown in **Figure 3c**, the calculated C_{dl} for Mo-NiO/Ni and NiO/Ni is 104 and 46 $mF \cdot cm^{-2}$ respectively, suggesting an increased electrochemically accessible interface, however, C_{dl} derived ECSA is only a qualitative proxy on porous/self-reconstructing NF electrodes and is therefore used here mainly for relative trend comparison. To verify the validity of the C_{dl} derived ECSA estimation, C_{dl} was measured in triplicate using independently prepared Mo-NiO/Ni electrodes under identical conditions, yielding 105, 104 and 105 mF cm^{-2} (average 104.7 $mF \cdot cm^{-2}$), confirming excellent reproducibility of the C_{dl} (and hence ECSA) values (Figure S7). The HER kinetics of Mo-NiO/Ni and NiO/Ni were evaluated by EIS. The spectra were fitted with a modified Randles circuit: L -

View Article Online
DOI: 10.1039/D5CY01487E

R_s - (R_{ct} ‖ CPE_{dl}) - (R_{ads} ‖ CPE_{ads}).(39) Here, R_s is the solution resistance, R_{ct} is the charge-transfer resistance, CPE_{dl} represents the non-ideal double-layer capacitance, and R_{ads} ‖ CPE_{ads} accounts for the low-frequency adsorption/desorption-related relaxation. The series L term reflects high-frequency inductive effects from instrumentation. The Nyquist plots of Mo-NiO/Ni sample exhibit a smaller Rct (6.6 Ω) than the NiO/Ni sample (393 Ω), Pt-C (21.5 Ω) and Ni foam (431 Ω), indicating that the Mo doping could considerably increase NiO/Ni charge transfer, as shown in **Figure 3d.** We note that Rct on 3D porous NF electrodes is an apparent, model-dependent parameter, therefore, we interpret the large R_{ct} decrease as a robust indicator of faster interfacial charge transfer only when consistent with the simultaneous improvements in overpotential, Tafel slope, and stability. The current density was adjusted by the ECSA to evaluate the intrinsic HER activity of the catalysts. As shown in **Figure S8**, the normalized polarization curves exhibit best HER performance of Mo-NiO/Ni. The findings propose that Mo doping boosts NiO/Ni intrinsic HER activity and catalytic active sites.

View Article Online
DOI: 10.1039/D5CY01487E

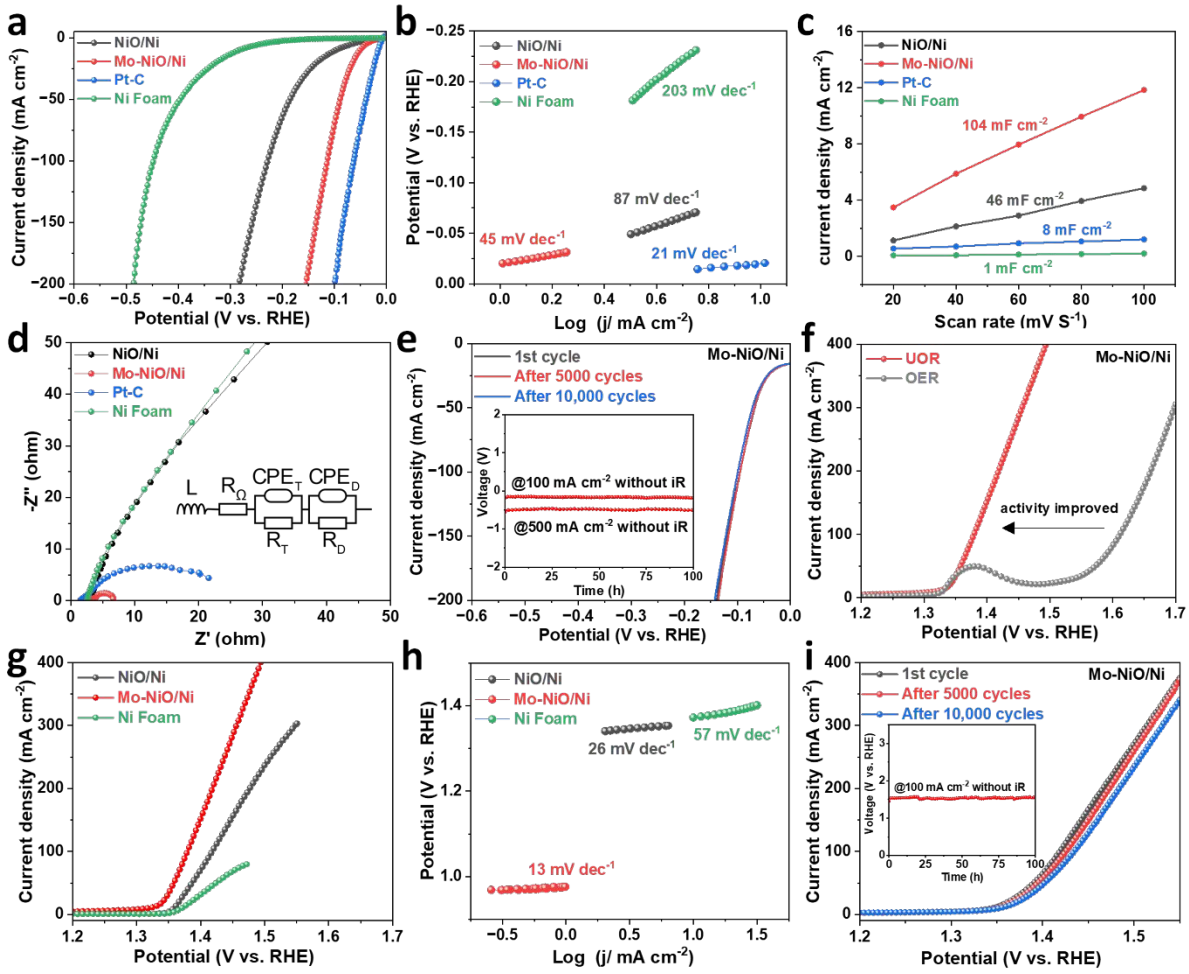

Figure 3. Electrochemical performance evaluation of Mo-NiO/Ni (a) compared LSV curves of different catalyst for HER. (b) corresponding Tafel plots. (c) double layered capacitance C_{dl} of the as prepared catalysts. (d) Nyquist plots for HER. (e) HER polarization curves after different CV cycles, inset is the chronopotentiometry curve at j of 500 and 100 mA·cm^{-2} (f) The oxidation performance comparison before and after the addition of urea. (g) LSV curves of different catalysts for UOR. (h) Corresponding Tafel plots towards UOR and (i), UOR polarization curves after different CV cycles, inset is the chronopotentiometry curve at current densities of 100 mA·cm^{-2} without iR compensation.

View Article Online
DOI: 10.1039/D5CY01487E

Along with catalytic activity, stability is a critical catalyst performance assessment. Thus, prolonged chronopotentiometry and CV cycles were used to determine Mo-NiO/Ni's durability in alkaline medium. **Figure 3e** shows that Mo-NiO/Ni has remarkable catalytic stability, with insignificant LSV curve alterations after 5,000 and 10,000 CV cycles during the HER process. Meanwhile, the stable chronopotentiometry curve recorded **(inset Figure 3e)** further illustrates the robustness of Mo-NiO/Ni in the alkaline electrocatalytic system. The Mo-NiO/Ni presents consistent performance over a duration of 100 h at high current densities of 500 and 100 $mA \cdot cm^{-2}$ in separate tests. This exceptional performance highlights the promising applicability of Mo-NiO/Ni in hydrogen production.

2.3 Electrocatalytic Urea oxidation reaction

The UOR activity of the as-prepared catalysts was assessed in 1 M KOH+0.5 M urea using a standard three-electrode configuration. Remarkably, the urea amount based UOR performance of Mo-NiO/Ni was first investigated in **Figure S9**. It can be found that Mo-NiO/Ni attains the better UOR activity at 0.5 M urea's concentration. **Figure 3f** shows that introducing 0.5 M urea to the electrolyte causes a substantial negative shift in the potentials Mo-NiO/Ni and a dramatic rise in current density. It should be noted that Ni-based anodes typically undergo in situ surface oxidation under anodic UOR polarization to form $Ni(OH)_2$/NiOOH-like species, which are widely regarded as the catalytically active surface, while the underlying NiO/Ni framework serves as a conductive scaffold.(40) In this system, UOR needs considerably smaller potential compared to OER, showing its inferior thermodynamic potential. **Figure 3g** illustrates the electrochemical LSV curves of NF, NiO/Ni and Mo-NiO/Ni in 1 M KOH+0.5 M urea. The Mo-NiO/Ni electrode exhibits superior electrocatalytic performance as compared to other catalysts. Specifically, the Mo-NiO/Ni electrode demonstrates anodic current densities of 10 and 100 $mA \cdot cm^{-2}$ at 1.31 and 1.37 V vs RHE,

View Article Online
DOI: 10.1039/D5CY01487E

respectively. These potentials are lower than those of NiO/Ni (1.35 and 1.41 V vs RHE) and NF (1.37 and 1.71 V vs RHE) at the same current densities. Furthermore, this catalyst requires only 1.53 V vs RHE to achieve a high current density of 500 $mA \cdot cm^{-2}$. Given the UOR equilibrium potential of 0.37 V *vs*. RHE, these values correspond to overpotentials of 0.94, 1.00, and 1.16 V at 10, 100, and 500 $mA \cdot cm^{-2}$, as depicted in **Figure S10,** respectively. The Tafel plot depicted in **Figure 3h** illustrates that the Tafel slope of Mo-NiO/Ni (13 $mV \cdot dec^{-1}$) is notably lower than that of NiO/Ni (26 $mV \cdot dec^{-1}$) and NF (57 $mV \cdot dec^{-1}$), indicating its superior electrocatalytic kinetics for the UOR. The analysis of EIS provides additional evidence of the material's effective electron transfer during the UOR process **Figure S11**. In Comparison to the previously published UOR catalyst, this sample exhibits a lower urea oxidation potential at a current density of 10 $mA \cdot cm^{-2}$, while also demonstrating more favorable kinetic performance, as illustrated in **Table S2**. Furthermore, we established that the optimal catalyst annealing temperature is at 450 °C for 2 hours, achieved through careful monitoring of the annealing temperature during the catalyst preparation process. For comparison, samples exposed 400 and 500 °C were also analyzed. These samples were evaluated based on their UOR performance and electrochemical impedance characteristics during the reaction process **Figure S12**. The ECSA of the catalysts was evaluated in urea containing electrolyte, utilizing the C_{dl} derived from CVs at different scan rates, as depicted in **Figure S13**. The C_{dl} value for the Mo-NiO/Ni catalyst is (102 $mF \cdot cm^{-2}$), substantially higher than that of NiO/Ni (22 $mF \cdot cm^{-2}$) and Ni foam (only 1 mF cm^{-2}). Figure 3i shows that Mo-NiO/Ni's catalytic stability during UOR is superior, as the LSV curves show no variations after 5,000 and 10,000 CV cycles. Meanwhile, the stable chronopotentiometry curve recorded **(inset Figure 3i)** further illustrates the robustness of Mo-NiO/Ni in 1 M KOH +0.5 M urea electrolyte. The Mo-NiO/Ni presents a consistent performance over a duration of 100 h at a high current density of 100

View Article Online
DOI: 10.1039/D5CY01487E

236 mA·cm^{-2}. These findings further validate the remarkable endurance of Mo-NiO/Ni in improving
237 long-term UOR performance.

238 Post HER and UOR characterization was evaluated via XRD, SEM, and XPS. The XRD
239 patterns **Figure S14** retain the characteristic reflections of NiO with no new crystalline impurity
240 phases detected, suggesting that the bulk NiO structure remains largely preserved. The
241 morphology result obtained after HER and UOR stability test **Figure S15** show well-preserved
242 confined nanoparticles, indicating the excellent mechanical stability of Mo-NiO/Ni. The XPS
243 spectra as depicted in **Figure S16** further show that Mo-NiO/Ni exhibits favorable stability.
244 Post-HER and UOR XPS analyses reveal the disappearance of the Ni^0 feature in the Ni 2p spectra
245 and the emergence of NiO diffraction peaks in XRD patterns, indicating electrochemically induced
246 surface reconstruction, under anodic UOR conditions the surface is expected to convert to
247 $Ni(OH)_2$/NiOOH-like species (ex situ XPS often appears predominantly Ni^{2+} after returning to
248 open circuit), whereas the NiO/Ni skeleton mainly provides electrical conductivity and structural
249 support. The coexistence of Ni^{2+} species and stable Mo signals confirms that Mo remains
250 associated with the reconstructed surface and/or subsurface, supporting its role in electronic
251 modulation/stabilization under operation.(41) Together, these results demonstrate excellent
252 structural and chemical stability and help rationalize the outstanding urea-assisted overall splitting
253 activity of Mo-NiO/Ni relative to current catalysts.

254 **2.4 Overall water and Urea splitting activity**

255 As shown in **Figure 4a**, two identical Mo-NiO/Ni electrodes were used as the cathode and
256 anode to test the practicality of water and urea splitting systems due to their strong bifunctional
257 catalytic activity for HER and UOR. Remarkably, this hybrid electrolyzer exhibits exceptional
258 performance on overall urea electrolysis under alkaline conditions, as illustrated in **Figure 4b**. It

View Article Online
DOI: 10.1039/D5CY01487E

achieves cell voltages of 1.33 and 1.62 V to attain current densities of 10 and 100 $mA \cdot cm^{-2}$ for urea-assisted electrolysis, compared with 1.50 and 1.82 V for overall water electrolysis under the same conditions. Thus, urea-assisted electrolysis reduces the required cell voltage by 170 mV at 10 $mA \cdot cm^{-2}$ and 200 mV at 100 $mA \cdot cm^{-2}$ relative to overall water splitting. Furthermore, this performance is competitive with other published electrocatalysts targeted urea-assisted water splitting, as detailed in **Table S3**. Moreover, at elevated current densities of 50, 100, and 150 $mA \cdot cm^{-2}$ are easily achieved at lower voltages of 1.51, 1.62 and 1.72 V, suppressing the overall water splitting system (1.7,1.82 and 1.92 V) as depicted in **Figure 4c**. This difference highlights the potential of the system for cost-effective hydrogen production and efficient treatment of urea-rich waste water. Further, long-term stability is also a vital factor for the practicality of any electrocatalyst. Significantly, the Mo-NiO/Ni electrode demonstrate remarkable stability, successfully catalyzing urea electrolysis for 100 hours without a noticeable decline in current density, as shown in **Figure 4d**. This observation highlights the catalyst excellent stability. Together, these results illustrate that the bifunctional Mo-NiO/Ni indeed exhibits highly efficient catalytic performance in the simultaneous processes of water and urea electrolysis, making it a promising candidate for hydrogen evolution applications.

View Article Online
DOI: 10.1039/D5CY01487E

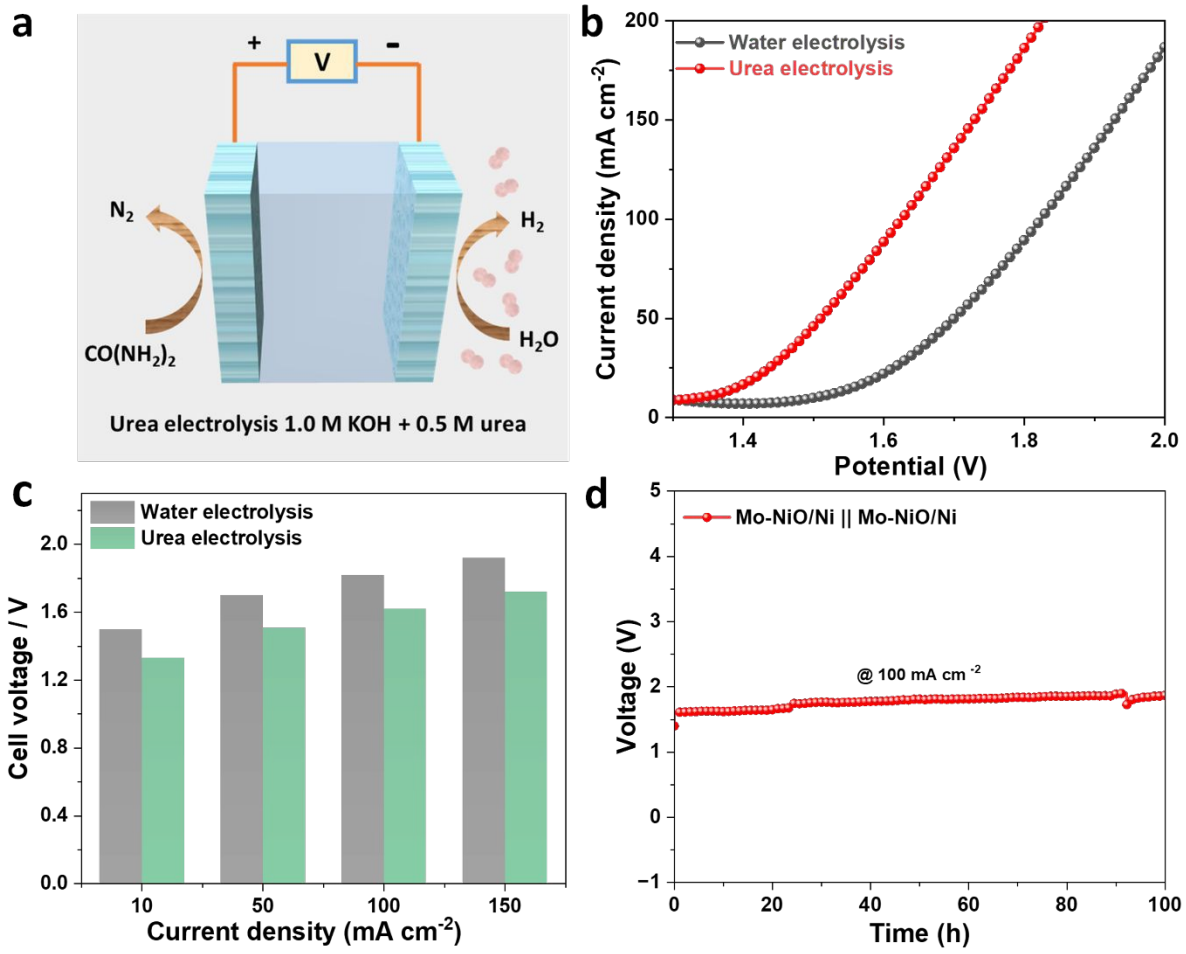

Figure 4. (a) Schematic illustration of the two-electrode system with Mo-NiO/Ni cathode and anode. (b) LSV curves of Mo-NiO/Ni || Mo-NiO/Ni under 1 M KOH and 1 M KOH having 0.5M urea (c) Comparison of cell voltages at 10, 50, 100 and 150 mA·cm^{-2} for water and urea electrolysis and (d) i-t curve at current density of 100 mA·cm^{-2}.

2.5 Study of catalytic mechanism

We note that the DFT models employed here represent idealized/static NiO/Ni and Mo-NiO/Ni interfaces. They do not explicitly include operando reconstruction (e.g., $Ni(OH)_2$/NiOOH formation), electrolyte/solvent, or applied potential, therefore, the calculations are used to provide qualitative trends in electronic redistribution and relative adsorption changes that are consistent with the experimental observations. DFT calculations were carried out to unravel the structural

View Article Online
DOI: 10.1039/D5CY01487E

and electronic modulation of the NiO/Ni interface upon Mo incorporation. As illustrated in **Figure 5a-b** Mo atoms are incorporated into the NiO lattice, inducing local lattice distortion and forming strong Mo-O-Ni bonds that alter the interfacial coordination environment. The corresponding charge density difference plot reveals significant electron redistribution, with pronounced electron accumulation near Mo sites and depletion around neighboring Ni atoms, indicating evident interfacial charge transfer as depicted in **Figure 5c**. The PDOS of NiO/Ni **Figure S17** exhibits dominant Ni 3d states near the Fermi level and strong Ni-O hybridization, consistent with partial metallicity at the interface. In contrast, Mo doping introduces additional Mo 4d electronic states near the Fermi level, effectively enhancing electronic conductivity and improving Mo-Ni-O hybridization, as illustrated in **Figure 5d**. This structural and electronic regulation optimizes the surface adsorption characteristics, promoting more efficient charge transfer and intermediate stabilization during catalytic reactions. Generally, the Gibbs free energy toward hydrogen adsorption (ΔG_{H*}) plays an important role in evaluating HER due to simultaneous optimized hydrogen adsorption/desorption reaction.(42, 43) The calculated Gibbs free-energy diagram deeper insights the catalytic role of Mo. As depicted in **Figure 5e,** the hydrogen adsorption free energy (ΔG_{H*}) of pristine NiO/Ni is -0.86 eV, indicating overly strong H binding, whereas Mo-NiO/Ni exhibits a near-thermoneutral ΔG_{H*} of 0.21 eV, suggesting more favorable HER kinetics. The HER structural models for NiO/Ni and Mo-NiO/Ni are illustrated in **Figure S18**. This near-thermoneutral hydrogen adsorption is consistent with the low HER overpotentials (51 and 113 mV at 10 and 100 $mA \cdot cm^{-2}$) and the reduced Tafel slope observed experimentally. Because UOR proceeds through multiple intermediates and parallel pathways, we use the dehydrogenation of adsorbed urea ($CO(NH_2)_2 \rightarrow CON_2$) as a representative potential-determining/rate-limiting step for comparative catalyst screening, rather than attempting to model the full operando network.

View Article Online
DOI: 10.1039/D5CY01487E

Furthermore, the calculated UOR free energy reaction pathway as illustrated in **Figure 5f,** indicates that Mo doping substantially decreases the energy barrier for this representative dehydrogenation step from 2.33 eV to 1.89 eV, facilitating the conversion of $*CO(NH_2)_2$ to $*CON_2$ intermediates. This lowered barrier is qualitatively consistent with the experimentally observed trend of a lower UOR onset potential and a smaller Tafel slope for Mo-NiO/Ni relative to NiO/Ni. DFT indicates that Mo-NiO/Ni **(Figure 5g)** and NiO/Ni **(Figure S19)** follow the same UOR route, where adsorbed urea is stepwise dehydrogenated and oxidized ($*CO(NH_2)_2 \rightarrow *CONH_2NH \rightarrow *CONHNH \rightarrow *CONNH \rightarrow *CON_2 \rightarrow *CO \rightarrow *COOH \rightarrow *CO_2$). Compared with NiO/Ni, Mo incorporation in Mo-NiO/Ni optimizes intermediate adsorption/stabilization, thereby promoting the overall UOR process. Collectively, these theoretical insights support that Mo modification optimizes the interfacial electronic structure and energetics of NiO/Ni, thereby promoting both hydrogen evolution and urea oxidation reactivity. These results indicate that Mo key role is to tune the electronic structure at the NiO/Ni interface, which is fundamentally different from bulk Ni-Mo-O/$NiMoO_x$ catalysts.

View Article Online
DOI: 10.1039/D5CY01487E

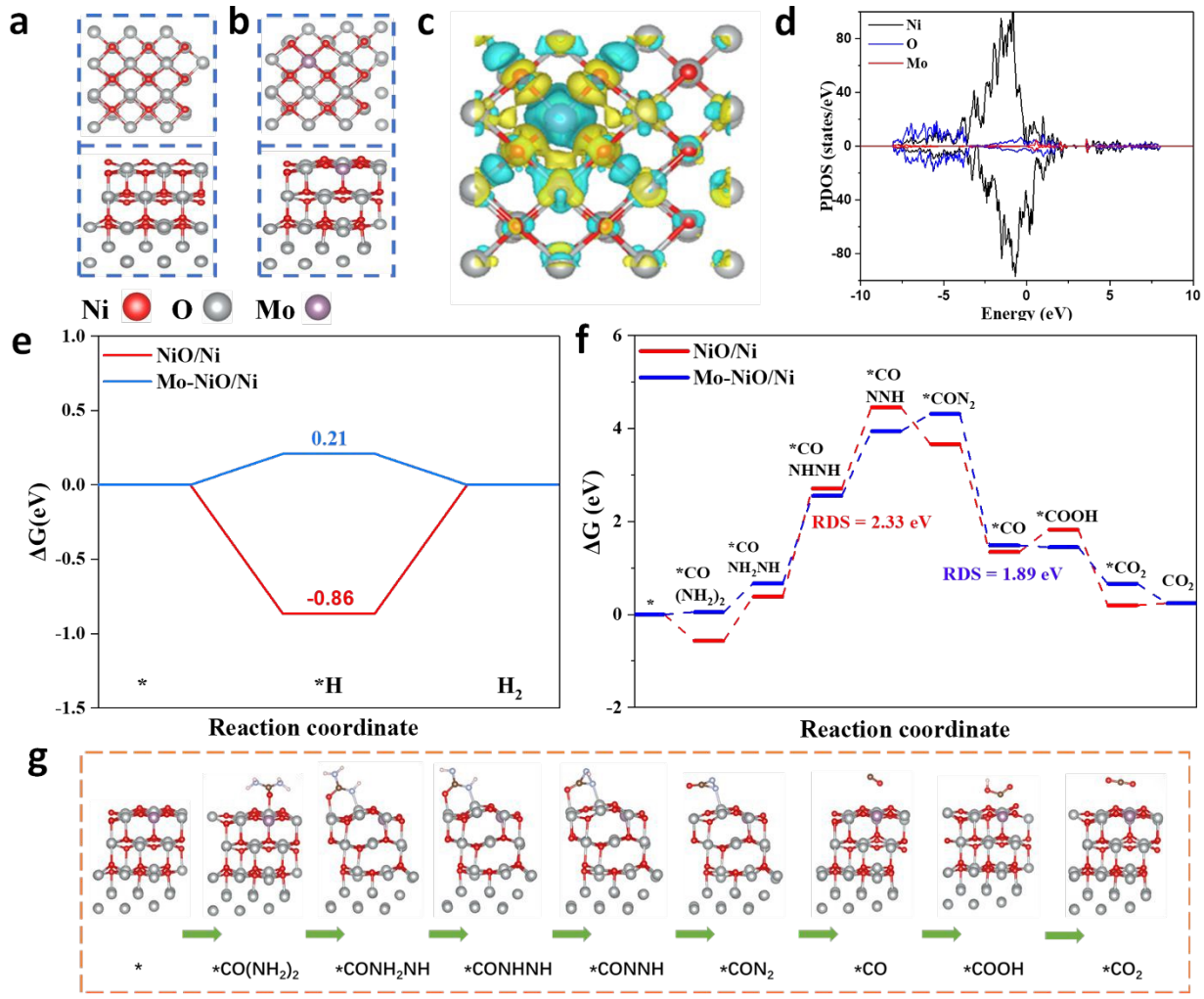

Figure 5. DFT calculations. a,b) Top and side view of structure models of (a) NiO/Ni, (b) Mo-NiO/Ni (c) Differential charge density of Mo-NiO/Ni. The yellow area signifies electron accumulation, whereas the cyan area indicates electron depletion (d) Calculated PDOS of Mo-NiO/Ni. (e) The Gibbs free energy diagram of HER for NiO/Ni and Mo-NiO/Ni. (f) Gibbs free-energy profile for UOR. (g) Diagrammatic representation of urea oxidation mechanism and its associated arrangements.

View Article Online
DOI: 10.1039/D5CY01487E

Conclusion

In conclusion, we have established a simple approach for the fabrication of an effective bifunctional Mo-NiO/Ni electrocatalyst by a one-step electrodeposition process followed by annealing. Remarkably, the prepared Mo-NiO/Ni catalyst achieves superior performance and prolonged stability for HER and UOR. The catalyst achieves HER η of 51 and 113 mV at 10 and 100 $mA \cdot cm^{-2}$, respectively, and a UOR potential of 1.37 V vs RHE to reach 100 $mA \cdot cm^{-2}$. A symmetric two-electrode electrolyzer demonstrates exceptional overall water and urea splitting performance, requiring 1.62 V at 100 $mA \cdot cm^{-2}$ in urea containing electrolyte, outperforming water electrolysis under identical conditions (1.82 V). DFT studies demonstrate that the Mo-NiO/Ni catalyst's strong bifunctional catalytic performance is mainly due to the electronic structure's modification, which improves conductivity and intermediate adsorption/desorption. Meanwhile, Mo-NiO/Ni uniformly grows on the NF and creates nanoparticles with more active sites for catalysis. This study presents a novel strategy for constructing high-performance Mo-NiO/Ni bifunctional catalysts, exhibits significant potential for industrial water splitting and urea oxidation.

Author contributions

Shahid Khan: Conceptualization, Methodology, Sample preparation, Electrochemical testing, Data analysis and Manuscript preparation. **Yang Lina**: Conducted DFT calculations. **Yafei Feng**: Formal analysis, Validation, Visualization. **Mingyu Cheng**: Formal analysis, Validation, Visualization. **Nazir Ahmad**: Formal analysis, Validation, Visualization. **Genqiang Zhang**: Supervised the project and contributed to the experimental planning, Data analysis and manuscript preparation.

Conflict of interest

View Article Online
DOI: 10.1039/D5CY01487E

The authors declare no conflict of interest.

Data Availability Statement

The data that support the findings of this study are available from the corresponding author upon reasonable request.

Acknowledgments

This work was supported by the financial support from the National Key R&D Program of China (2022YFA1504001), the National Natural Science Foundation of China (T2325021, 22321001), the CAS Project for Young Scientists in Basic Research (YSBR-070). The numerical calculations in this paper have been done in the Supercomputing Center of University of science and Technology of China.

View Article Online
DOI: 10.1039/D5CY01487E

References

1. Jian J, Qiao Y, Chen F, Liu C, Liu W, Li Z, et al. Local Charge Density Regulation of NiP_2 Nanosheets via Ru Doping for Electrocatalytic Urea Oxidation. Applied Catalysis B: Environment and Energy. 2025:125390.
2. Yu H, Zhu S, Hao Y, Chang YM, Li L, Ma J, et al. Modulating local interfacial bonding environment of heterostructures for energy-saving hydrogen production at high current densities. Advanced Functional Materials. 2023;33(12):2212811.
3. Xiang W, Yang N, Li X, Linnemann J, Hagemann U, Ruediger O, et al. 3D atomic-scale imaging of mixed Co-Fe spinel oxide nanoparticles during oxygen evolution reaction. Nature Communications. 2022;13(1):179.
4. Wang X, Xi S, Huang P, Du Y, Zhong H, Wang Q, et al. Pivotal role of reversible NiO_6 geometric conversion in oxygen evolution. Nature. 2022;611(7937):702-8.
5. Zhu B, Liang Z, Zou R. Designing advanced catalysts for energy conversion based on urea oxidation reaction. Small. 2020;16(7):1906133.
6. Wang L, Zhu Y, Wen Y, Li S, Cui C, Ni F, et al. Regulating the local charge distribution of Ni active sites for the urea oxidation reaction. Angewandte Chemie International Edition. 2021;60(19):10577-82.
7. Hu X, Zhu J, Li J, Wu Q. Urea electrooxidation: current development and understanding of Ni-based catalysts. ChemElectroChem. 2020;7(15):3211-28.
8. Boggs BK, King RL, Botte GG. Urea electrolysis: direct hydrogen production from urine. Chemical Communications. 2009(32):4859-61.
9. Geng S-K, Zheng Y, Li S-Q, Su H, Zhao X, Hu J, et al. Nickel ferrocyanide as a high-performance urea oxidation electrocatalyst. Nature Energy. 2021;6(9):904-12.

View Article Online
DOI: 10.1039/D5CY01487E

10. Jiang H, Sun M, Wu S, Huang B, Lee CS, Zhang W. Oxygen-incorporated NiMoP nanotube arrays as efficient bifunctional electrocatalysts for urea-assisted energy-saving hydrogen production in alkaline electrolyte. Advanced Functional Materials. 2021;31(43):2104951.
11. Kumar A, Liu X, Lee J, Debnath B, Jadhav AR, Shao X, et al. Discovering ultrahigh loading of single-metal-atoms via surface tensile-strain for unprecedented urea electrolysis. Energy & Environmental Science. 2021;14(12):6494-505.
12. Roger I, Shipman MA, Symes MD. Earth-abundant catalysts for electrochemical and photoelectrochemical water splitting. Nature Reviews Chemistry. 2017;1(1):0003.
13. Gong M, Dai H. A mini review of NiFe-based materials as highly active oxygen evolution reaction electrocatalysts. Nano Research. 2015;8(1):23-39.
14. McCrory CC, Jung S, Peters JC, Jaramillo TF. Benchmarking heterogeneous electrocatalysts for the oxygen evolution reaction. Journal of the American Chemical Society. 2013;135(45):16977-87.
15. Babar P, Lokhande A, Karade V, Pawar B, Gang MG, Pawar S, et al. Bifunctional 2D electrocatalysts of transition metal hydroxide nanosheet arrays for water splitting and urea electrolysis. ACS Sustainable Chemistry & Engineering. 2019;7(11):10035-43.
16. Xu C, Yang X, Li S, Li K, Xi B, Han Q-W, et al. Modulating the electronic configuration of Co species in MOF/MXene nanosheet derived Co-based mixed spinel oxides for an efficient oxygen evolution reaction. Inorganic Chemistry Frontiers. 2023;10(1):85-92.
17. Zhu W, Yue Z, Zhang W, Hu N, Luo Z, Ren M, et al. Wet-chemistry topotactic synthesis of bimetallic iron–nickel sulfide nanoarrays: an advanced and versatile catalyst for energy efficient overall water and urea electrolysis. Journal of Materials Chemistry A. 2018;6(10):4346-53.

View Article Online
DOI: 10.1039/D5CY01487E

18. Han N, Liu P, Jiang J, Ai L, Shao Z, Liu S. Recent advances in nanostructured metal nitrides for water splitting. Journal of Materials Chemistry A. 2018;6(41):19912-33.

19. Cao W, Shen Q, Men D, Ouyang B, Sun Y, Xu K. Phase engineering of iron group transition metal selenides for water splitting. Materials Chemistry Frontiers 2023;7(20):4865-79.

20. Wang Z, Yang J, Wang W, Zhou F, Zhou H, Xue Z, et al. Hollow cobalt-nickel phosphide nanocages for efficient electrochemical overall water splitting. Science China Material. 2021;64(4):861-9.

21. Chen Z, Song Y, Cai J, Zheng X, Han D, Wu Y, et al. Tailoring the d-band centers enables Co4N nanosheets to be highly active for hydrogen evolution catalysis. Angewandte Chemie International Edition. 2018;57(18):5076-80.

22. Yao N, Li P, Zhou Z, Zhao Y, Cheng G, Chen S, et al. Synergistically tuning water and hydrogen binding abilities over Co_4N by Cr doping for exceptional alkaline hydrogen evolution electrocatalysis. Advanced Energy Materials. 2019;9(41):1902449.

23. Zhao J, Zhang Y, Guo H, Ren J, Zhang H, Wu Y, et al. Defect-rich $Ni(OH)_2$/NiO regulated by WO_3 as core–shell nanoarrays achieving energy-saving water-to-hydrogen conversion via urea electrolysis. Chemical Engineering Journal. 2022;433:134497.

24. Rao NN, Alex C, Tomar S, Kovilakath MSN, Lee S-C, Bhattacharjee S, et al. Interface-driven electrocatalysis: Highlighting the role of $NdNiO_3$-NiO heterointerface in urea electro-oxidation. Applied Catalysis B: Environment and Energy. 2025;371:125177.

25. Kou T, Chen M, Wu F, Smart TJ, Wang S, Wu Y, et al. Carbon doping switching on the hydrogen adsorption activity of NiO for hydrogen evolution reaction. Nature communications. 2020;11(1):590.

View Article Online
DOI: 10.1039/D5CY01487E

26. Cai F, Liao L, Zhao Y, Li D, Zeng J, Yu F, et al. Large-current-stable bifunctional nanoporous Fe-rich nitride electrocatalysts for highly efficient overall water and urea splitting. Journal of Materials Chemistry A. 2021;9(16):10199-207.

27. Yu Z-Y, Lang C-C, Gao M-R, Chen Y, Fu Q-Q, Duan Y, et al. Ni–Mo–O nanorod-derived composite catalysts for efficient alkaline water-to-hydrogen conversion via urea electrolysis. Energy & Environmental Science. 2018;11(7):1890-7.

28. Wang C, Lu H, Mao Z, Yan C, Shen G, Wang X. Bimetal Schottky heterojunction boosting energy-saving hydrogen production from alkaline water via urea electrocatalysis. Advanced Functional Materials. 2020;30(21):2000556.

29. Zhu X, Dou X, Dai J, An X, Guo Y, Zhang L, et al. Metallic nickel hydroxide nanosheets give superior electrocatalytic oxidation of urea for fuel cells. Angewandte Chemie International Edition. 2016;55(40):12465-9.

30. He Q, Wan Y, Jiang H, Pan Z, Wu C, Wang M, et al. Nickel vacancies boost reconstruction in nickel hydroxide electrocatalyst. ACS Energy Letters. 2018;3(6):1373-80.

31. Maheskumar V, Min A, Moon CJ, Senthil RA, Choi MY. Modulating the electronic structure of Ni/NiO nanocomposite with high-valence Mo doping for energy-saving hydrogen production via boosting urea oxidation kinetics. Small Structures. 2023;4(12):2300212.

32. Wang T, Wu H, Feng C, Ding Y, Mei H. Ni, N-codoped $NiMoO_4$ grown on 3D nickel foam as bifunctional electrocatalysts for hydrogen production in urea-water electrolysis. Electrochimica Acta. 2021;391:138931.

33. Ali T, Wang X, Tang K, Li Q, Sajjad S, Khan S, et al. SnS_2 quantum dots growth on MoS_2: Atomic-level heterostructure for electrocatalytic hydrogen evolution. Electrochimica Acta. 2019;300:45-52.

View Article Online
DOI: 10.1039/D5CY01487E

34. Yang C, Gao N, Wang X, Lu J, Cao L, Li Y, et al. Stable and efficient seawater splitting on a porous phosphate-intercalated NiFe (oxy) hydroxide@$NiMoO_4$ core-shell micropillar electrode. Energy Materials. 2021;1(2):N/A-N/A.

35. Zhu Y, Zhang J, Qian Q, Li Y, Li Z, Liu Y, et al. Dual nanoislands on Ni/C hybrid nanosheet activate superior hydrazine oxidation-assisted high-efficiency H_2 production. Angewandte Chemie International Edition. 2022;61(2):e202113082.

36. Kotsis K, Staemmler V. Ab initio calculations of the O1s XPS spectra of ZnO and Zn oxo compounds. Physical Chemistry Chemical Physics. 2006;8(13):1490-8.

37. Tanhaei M, Yang M, Cheng JJ, Ren Y, Nemati A, Pan J, et al. Enhanced CO_2 sorption in a hybrid PEI-Mo oxide film via pulsed electrodeposition. Materials Advances. 2022;3(13):5510-20.

38. Sun H, Lian Y, Yang C, Xiong L, Qi P, Mu Q, et al. A hierarchical nickel-carbon structure templated by metal-organic frameworks for efficient overall water splitting. Energy & Environmental Science. 2018;11(9):2363-71.

39. Ali T, Qiao W, Zhang D, Liu W, Sajjad S, Yan C, et al. Surface sulfur vacancy engineering of metal sulfides promoted desorption of hydrogen atoms for enhanced electrocatalytic hydrogen evolution. The Journal of Physical Chemistry C. 2021;125(23):12707-12.

40. Guo X, Qiu L, Li M, Tian F, Ren X, Jie S, et al. Accelerating the generation of NiOOH by in-situ surface phosphating nickel sulfide for promoting the proton-coupled electron transfer kinetics of urea electrolysis. Chemical Engineering Journal. 2024;483:149264.

41. Luo J, Zhang Y, Tang L, Lu D, Zhang T, Zhao H, et al. Electrochemical self-reconstruction helps self-supported Ni_3S_2@ NiFeOOH-MOF/NFF electrodes to enhance electrocatalytic oxygen evolution. International Journal of Hydrogen Energy. 2025;114:394-402.

View Article Online
DOI: 10.1039/D5CY01487E

42. Li Y, Zhang J, Liu Y, Qian Q, Li Z, Zhu Y, et al. Partially exposed RuP_2 surface in hybrid structure endows its bifunctionality for hydrazine oxidation and hydrogen evolution catalysis. Science advances. 2020;6(44):eabb4197.

43. Qian Q, Li Y, Liu Y, Zhang G. General anion-exchange reaction derived amorphous mixed-metal oxides hollow nanoprisms for highly efficient water oxidation electrocatalysis. Applied Catalysis B: Environmental. 2020;266:118642.

View Article Online
DOI: 10.1039/D5CY01487E

Data Availability Statement

The data that support the findings of this study are available from the corresponding author upon reasonable request.